Recent Progress in Tailoring Trap-based Positron Beams

M. R. Natisin, N. C. Hurst, J. R. Danielson and C. M. Surko

Physics Department, University of California, San Diego
La Jolla CA 92093-0319, USA

Abstract. Recent progress is described to implement two approaches to specially tailor trap-based positron beams. Experiments and simulations are presented to understand the limits on the energy spread and pulse duration of positron beams extracted from a Penning-Malmberg (PM) trap after the particles have been buffer-gas cooled (or heated) in the range of temperatures $1000 \geq T \geq 300$ K. These simulations are also used to predict beam performance for cryogenically cooled positrons. Experiments and simulations are also presented to understand the properties of beams formed when plasmas are tailored in a PM trap in a 5 tesla magnetic field, then non-adiabatically extracted from the field using a specially designed high-permeability grid to create a new class of electrostatically guided beams.

INTRODUCTION

Low-energy positrons and antiprotons (e.g., with energies $\sim 10^{-4} - 10$ eV) are important in many areas of science and technology. One example is studies of positron binding to ordinary matter (a key element of an "antimatter-matter chemistry") and its implications for positron annihilation in a variety of media [1-5]. Another is the creation and study of antihydrogen [6-9] to test fundamental symmetries of nature such as the CPT theorem. A third is the quest to create a BEC gas of positronium atoms [10, 11]; that, in turn, is expected to potentially enable the creation of an annihilation gamma-ray laser [12]. Further development of tailored positron sources also holds promise for other applications. In medicine, for example, uses of positrons include positron emission tomography (PET), to study human metabolic processes [13], and also in drug design in conjunction with animal studies [14]. There is also a wealth of applications of low-energy positrons in materials science [2, 15].

Antimatter can be stored indefinitely in the form of single component plasmas (SCP) in electromagnetic [i.e., Penning-Malmberg (PM)] traps. Plasmas can be cooled and manipulated, to then be released in tailored beams of antiparticles. The conventional approach to antihydrogen formation works in a similar manner using tailored positron and antiproton plasmas [6, 7]. Here we exploit this trapping technology to develop new methods to create specially tailored positron beams for a range of applications.

Trap-based, magnetically guided positron beams [16] have proven enormously

useful for positron-atomic physics and materials studies, and for fundamental physics such as the creation of a Ps BEC [10, 12]. On the other hand, electrostatic positron beams (i.e., beams in regions where the magnetic field $B = 0$) are desirable in that they can be further brightness-enhanced using electrostatic focusing and "remoderation" techniques (i.e., taking energy out of the particles in inelastic collisions at a material surface [17]). Described here is work to further improve both magnetically guided and electrostatic positron beams.

TWO APPROACHES TO IMPROVED POSITRON BEAMS

Extraction of Colder Beams from a Buffer-gas Trap

The now-conventional laboratory source of low energy positrons is the radioisotope ^{22}Na, followed by a solid neon "moderator" and a buffer-gas accumulator [18]. The moderator slows positrons to eV energies, feeding an accumulator which consists of a multiple-stage (e.g., three stages at UCSD) PM trap in a ~ 0.1 T field [19, 20]. Inelastic collisions with N_2 molecules in the three differentially pumped stages slow the positrons enough for them to be trapped in the third stage, where they cool to 300 K in ≤ 0.05 s by inelastic collisions with both N_2 and CF_4 molecules. The typical trapping efficiency of ~ 10 - 30 % is the best achieved by any technique to date by more than a factor of 10. The positron lifetime ($\sim$ tens of seconds) is limited by annihilation on the buffer gas. With the buffer gas removed, the positron lifetime can be hours or longer, depending upon the base pressure in the device.

Using 300 K buffer gases, we developed a method to create positron beams with energy resolution ~ 45 meV FWHM (i.e., $\Delta E_\parallel = 18$ meV; $\Delta E_\perp = 25$ meV) and pulse duration τ of ~ 2 μs FWHM, tunable from 50 meV to many tens of electron volts [16]. Positrons, which have been cooled in the PM trap, are then forced over a fixed exit-gate barrier by carefully raising the bottom of the trapping well (see below). These beams have had enormous impact in positron-atomic physics [1, 3-5].

The positron ejection process involves a central "well" electrode with two adjacent "wall" electrodes. One of the confining electrodes is biased strongly repulsive, while the other, exit-gate electrode, is set to a potential that defines the final beam energy. The central well electrode potential is then raised until the positrons overcome the exit-gate barrier and are released from the trap.

Recently, we conducted new experiments and used particle simulations to better understand the limits on energy resolution and minimum pulse duration resulting from this injection process. While the perpendicular energy spread is set by the buffer gas temperature, the parallel energy distribution and pulse duration are set by the dynamics of the release process. At a given positron temperature, a slower rate of increase of the well potential results in a narrower parallel energy spread, but a longer pulse duration. Conversely, the pulse duration can be shortened by forcing the particles out faster, but results in a broader parallel energy spread. Many applications benefit from short pulses *and* narrow energy spreads, thus motivating the present studies.

Monte Carlo techniques are used to simulate the positions and velocities of the

particles as they interact with the time dependent electric fields during the injection process. All electric fields are due to externally applied potentials. The simulation starts with ~ 10,000 particles in a Boltzmann parallel energy distribution, and an axial distribution determined by the trapping well. The potential as a function of time is determined by solving the Laplace equation everywhere in space using the finite element method (FEM) and the actual electrode geometry. These solutions are interpolated to find the potential every 50 ns. The position and velocity of each particle is found every 10 ns by numerically integrating the Lorentz force equation. Radial effects are estimated to be of order a couple percent, and so only on-axis potential solutions are described. Due to the small numbers of positrons involved, particle-particle interactions, interactions with background gas molecules, and plasma effects are neglected.

The results of the simulations are shown in Fig. 1. They demonstrate that the beam formation process is intrinsically dynamical. Figs. 1 (a-c) show the particle distribution in space at three times as the particles are ejected. Figs. 1 (d-f) show, respectively: the time dependence of the fraction of particles in the well, the well width, and the effective temperature of the particles in the well, during the ejection process. As the well potential is raised, the effective well width, as seen by the positrons, increases. This results in significant adiabatic cooling while the particles are still confined in the potential well, as shown in the right panel of Fig. 1.

Figure 1 also shows an increase in the cooling rate following the adiabatic cooling. Instead of evaporative cooling, this more rapid cooling appears to correlate better with an increased well expansion rate rather than with particle loss. This cooling competes with increased particle acceleration and heating due to the increased effect of the potential on the electrode opposite the exit gate as the central well potential is raised.
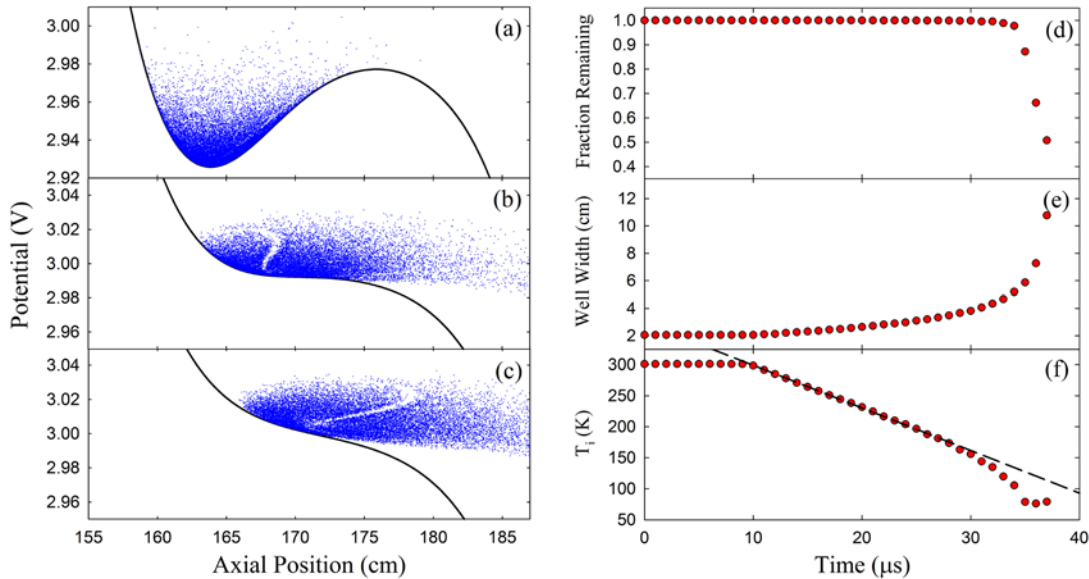

FIGURE 1. Simulation results for the electrical potentials and particle positions during the formation of a 300K positron beam at times (a) t = 35, (b) t = 38 and (c) t = 39 μs after the start of the ramp; and various parameters as a function of time; (d) fraction of particles remaining; (e) potential well width as seen by a positron with energy $T_i/2$, and (f) parallel temperature of the remaining positrons in the well.

The key beam parameters are the parallel energy spread $\Delta E_\parallel$ and the pulse duration τ. Figure 2 compares the simulated and experimental parallel energy (a), and time distribution (b), for a 2 eV beam formed by positrons with an initial temperature of 300 K. The well is raised using an RC ramp with a rise time (10 to 90%) of 33.3 μs and a final (steady-state) voltage of 0.5 V above the exit-gate voltage. The predicted and measured parallel energy spreads are 24.4 and 24.0 meV, with pulse durations of 1.81 and 1.82 μs, respectively.

The two variables, $\Delta E_\parallel$ and τ, depend upon the ramp rate and initial positron temperature T_i. The dependence of the energy spread on T_i is shown in Fig. 3 (a), for both the simulation and experiment. It can be seen that, as the initial positron temperature is reduced, the energy spread of the final beam is also reduced. The pulse duration (not shown) displays similar behavior. While both the energy spread and pulse duration have different dependences on the initial temperature, the combination $\tau\Delta E_\parallel$ is proportional to T_i for a fixed ramp rate (cf., Fig. 3b). This means that, if the positrons can be further cooled before injection, both the energy and time resolution of the final beam can be improved.
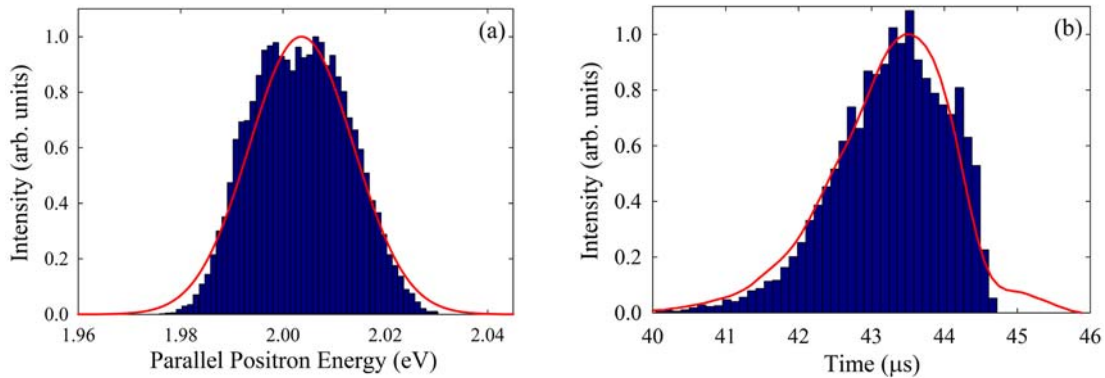

FIGURE 2. (a) the parallel energy distribution and (b) time distribution of beam pulses. Blue bars are from the simulation, and the red curves are experimental results.
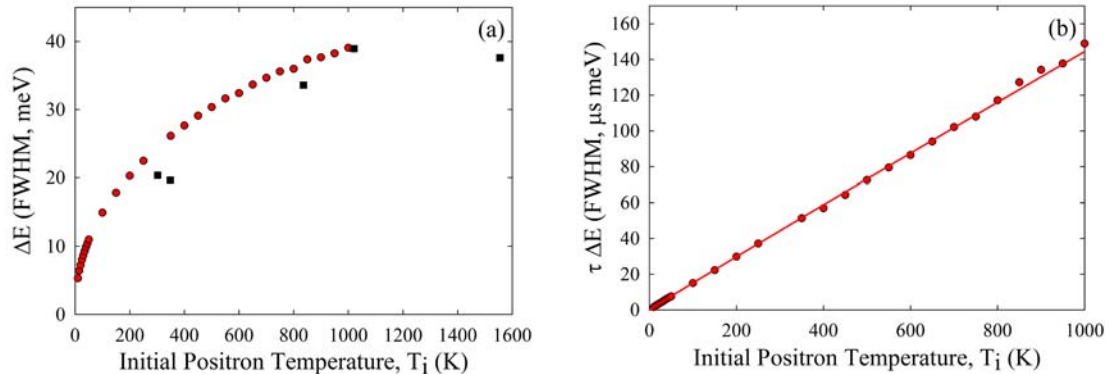

FIGURE 3. Vary initial positron temperature with fixed ramp rate showing dependence of (a) parallel energy spread and (b) product of parallel energy spread and pulse duration. Red circles are simulation and black squares are experimental results. Solid red line is a power law fit giving $\tau\Delta E_\parallel = 0.167\ T_i^{0.98}$.

If T_i is held fixed, decreasing the ramp rate will decrease $\Delta E_\parallel$ and increase τ. Thus, lowering the temperature *and* decreasing the ramp rate provides an additional gain in energy resolution. If this is done in such a way as to maintain a fixed τ, a linear decrease in energy spread with decreasing temperature can be achieved. The origins of the dependence of $\Delta E_\parallel$ and τ on T_i are the subject of continuing study. Nevertheless, the results thus far prepare us to conduct new experiments to improve beam performance using a cryogenically cooled buffer gas. In particular, we will exploit the fact that $\Delta E_\parallel$ decreases linearly with T_i, if τ is kept constant by increasing the ramp rate.

We have a cryo-cooler with large cooling capacity (Cryomech, Model AL325; 230 W cooling power at 50 K) that is ideal for this application. We plan to build a separate, cold, trapping stage and begin experiments to develop such a cold beam. First choices for a cooling gas will be either N_2, CF_4 or a mixture of the two, based both on previous experience, work modeling the buffer-gas cooling process [21], and the temperature-vapor pressure curves for these gases.

The goal will be to cool positrons to ≤ 50 K. The simulations indicate that this will permit the creation of a beam with a total energy spread $\Delta E_{tot} \leq 9$ meV FWHM with an acceptable temporal pulse width $\boldsymbol{\tau} = 2$ μs. If successful, this beam will enable, for example, dramatic improvements in the ability to resolve specific vibrations involved in resonant positron annihilation on molecules and a much-improved ability to study a variety of threshold phenomena in atomic physics [1, 5].

The ultimate limit of the energy resolution ΔE using a cryogenic buffer gas for cooling is unclear. Efficient cooling at low temperatures can be done most easily by exciting molecular rotations [22]. While N_2 and SF_4 will freeze out at temperatures significantly less than ~ 40 K, other cooling gases could be considered. Unfortunately, while it has an acceptable vapor pressure at much lower temperature, the lowest energy rotational mode in H_2 is ~ 90 K, and so cooling to low temperatures is problematic, even if D_2 were used. An intriguing possibility is to exploit the dimerization of noble gas atoms. Judging from vapor pressure curves, Ne might be a good candidate as the vapor pressure is acceptably high at $T \leq 20$ K and the dimer binding energy is ~ 40 K. In this case, one could use H_2 to cool to ≤ 100 K and neon dimers to cool to $T \leq 20$ K.

Extraction of Small Beams from Plasmas in a HF Trap

The second beam-formation technology we wish to exploit involves cyclotron-cooled particles in a high-field PM trap. Here, we utilize the fact that the space charge potential of a single component plasma is highest on the magnetic axis. As illustrated schematically in Fig. 4, if the confining potential is lowered, the first particles to escape are those closest to the axis of symmetry. Pulsed beams are extracted by carefully lowering the exit-gate potential for a brief period, $\Delta t \sim 10$ μs. This technique was exploited to create beams with small transverse spatial extent and energy spreads comparable to the temperature of the parent plasma that was confined in a PM trap in a 5 tesla field [23-25]. An important goal is to further develop this technique.

Many applications require electrostatic beams [3, 26]; since, as mentioned above, techniques such as "remoderation" [27] can then be used for further brightness

enhancement. The focus of current work is the extraction of high-quality electrostatic beams from the 5 tesla PM trap. Due to conservation of canonical momentum, particles gain perpendicular velocity during non-adiabatic extraction according to the formula $\delta v_\perp = (eB/2mc)r$, where r is the particle's radial position from the beam axis, and B the field at the extraction point. These perpendicular velocity "kicks" are detrimental to beam divergence and focusing properties, therefore the primary challenge is to reduce the kick magnitude. The strategy is to guide the beam adiabaticaly to low B, then perform a nonadiabatic extraction from the field. The minimum B field before extraction is chosen such that the transverse beam extent is still acceptably small.

In the high-magnetic-field region, it has been shown theoretically and confirmed with experiments that, for sufficiently small amplitude beams, the radial profile of the beam is a Gaussian, with a width $\rho_b \propto \lambda_D$, the Debye length [24]. Since $\lambda_D \propto \sqrt{T/n}$, narrow beams can be created with high efficiency by extracting the particles from cold, dense plasmas.
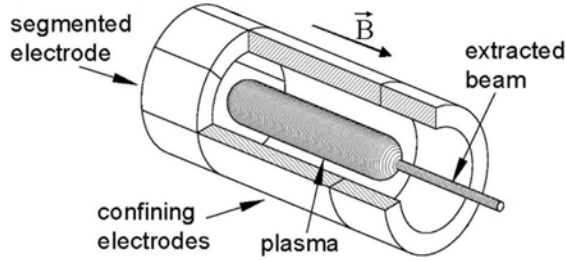

FIGURE 4. Cartoon of the arrangement to extract small beams from a PM trap. For the work described here, B = 5 T.

The nature of the radial beam profiles and the beam energy distributions was also investigated. Theoretical expressions were developed for these and other beam parameters [24, 25]. The key parameter determining the beam properties is the scaled beam amplitude ξ, from which the beam radius ρ_b can be obtained,

$$\xi \equiv (N_b/N_0)(r_p/2\lambda_D)^2 = (e\Delta\phi/T); \qquad \rho_b = 2\lambda_D[1+\xi]^{1/2} \qquad (1)$$

where N_b is the number extracted from plasma of N_0 particles, and $\Delta\phi$ is the change in the space charge potential across the beam due to the pulsed extraction. The measured energy distributions compare well with the predictions of the theory. It was also shown that, for $\xi \leq 1$, the energy spread of the extracted beam pulses is comparable to the plasma temperature T [25].

In order to get the extracted beam into a field-free region, a new experiment was constructed, as illustrated in Fig 5. Here, electrons (used in place of positrons for increased data rate) are compressed and cooled in a 5 T PM trap (stage I) and guided adiabatically out of the magnet to a field of ~ 10 - 50 gauss (stage II) [28]. The natural falloff of the HF magnet is augmented by an opposing solenoid and then by a discrete opposing coil. Particles are extracted from the field non-adiabatically, through a hole in a Permalloy plate [20], into the Permalloy-shielded region (stage III), also shown in Fig. 5. In this magnetic-field-free region, the particles are focused electrostatically into an axially movable collector cup through an aperture with diameter 2.4 mm. Shown in

Fig. 6 is an example of the collector-cup signal I_s as a function of collector position, for a fixed lens voltage of 5 kV [28].
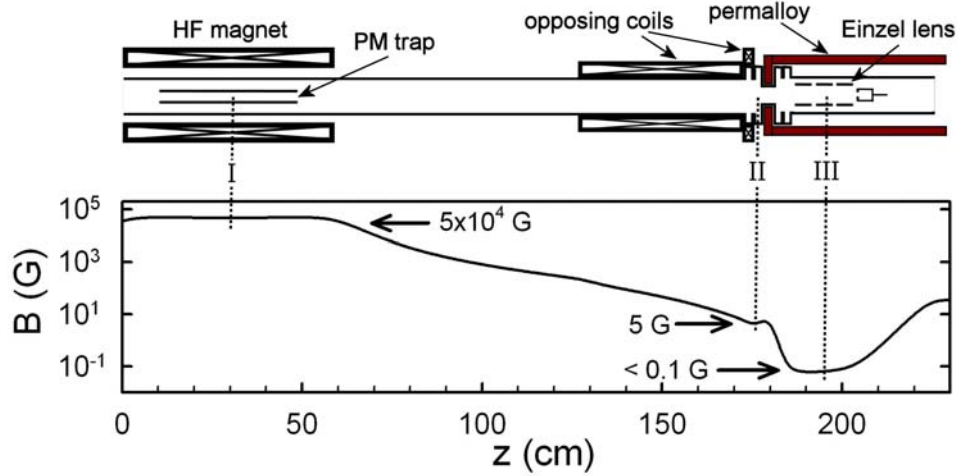

FIGURE 5. Schematic diagram of the apparatus to extract specially tailored beams from the high-field (5 T) PM trap into a field-free region. Stages I – III of the extraction process are indicated.

Expressions were derived for the properties of the extracted beams including perpendicular energy and perpendicular energy spread and the dispersion in parallel and perpendicular energies. Useful analytic expressions could be derived assuming a Gaussian radial beam profile and extraction from trapped plasma with a Maxwellian velocity distribution. A key result is an analytic expression for the invariant beam emittance ε* that is valid *both* in the regime in which the extraction momentum kick dominates and in the regime in which the plasma temperature is dominant. In the units defined here,

$$\epsilon^* \equiv \left(\overline{r^2} \bar{E}_{\perp f} \right)^{1/2} = \rho_b \sqrt{T} \sqrt{1 + \left(\frac{\rho_b}{2\rho_c} \right)^2} \tag{2}$$

where ρ_c is the cyclotron radius. While similar expressions appear in the literature [20, 29], to our knowledge, this is the first expression that connects the two regimes using self-consistent assumptions.

Simulations were also conducted to predict the beam properties as it propagates through the electrostatic lens [28]. The results are shown by the red cross-hatched regions in Fig. 6. The spread in the predictions takes into account uncertainty in beam radius at the extraction point. The experimental results are in reasonable agreement with the lower boundary of the simulations. The effects of lens aberrations on the focal-plane image were also investigated [28].

These results give us confidence that we have a quantitative understanding of the parameters of the extracted electrostatic beams. However, a remaining goal is to develop an effective way to further mitigate the extraction velocity kicks.
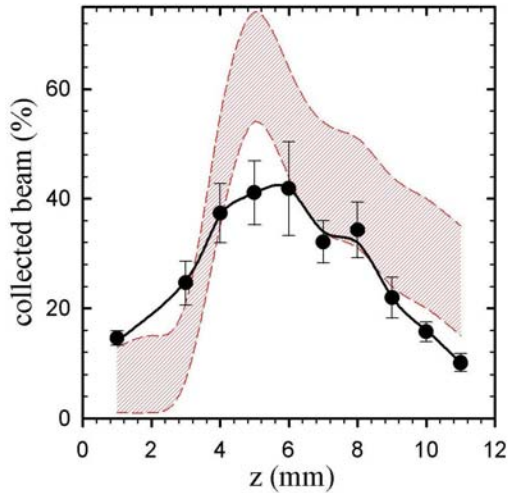
FIGURE 6. Fraction of the electrostatic beam collected as a function of collector position, with 5 kV lens voltage. The red stippled regions are the predictions of computer simulations taking into account the experimental uncertainties. See Ref. [28] for details.

Wolfgang Stoeffl and collaborators at Lawrence Livermore National Laboratory developed a high-permeability extraction grid (with tapered radial spokes; shown in Fig. 7) to minimize the kicks [30]. This grid, referred to as "magnetic spider" was placed in the hole in the Permalloy plate that we used previously. The purpose of the spider is to reduce the scale length of the changing magnetic field at the point of field-extraction. As mentioned above, the kick particles experience upon extraction from the spider can be approximated using $\delta v_\perp = (eB/2mc)r$, with the dimension r, previously ~ 4.5 mm now $d/4 \sim 0.25$ mm, where d is the mean width of the open area between spokes averaged over the radial beam profile. In principle this can reduce the mean kicks by an order of magnitude. Experiments were conducted recently with a variety of beam energies from 15 to 35 eV and magnetic fields B_s at the spider as low as 5 G. These experimental results were augmented by the results of simulations. Measured performance was in approximate agreement with expectations for $B_s \geq 30$ G; however, as shown in Fig. 7 (right panel), at lower B_s, performance was degraded. While not completely certain at this point, the data are consistent with a magnetic field transverse to the face of the spider of ~ 0.2 G, possibly due to slight misalignment between field and apparatus. To optimize spider performance, we must better understand and mitigate this effect.
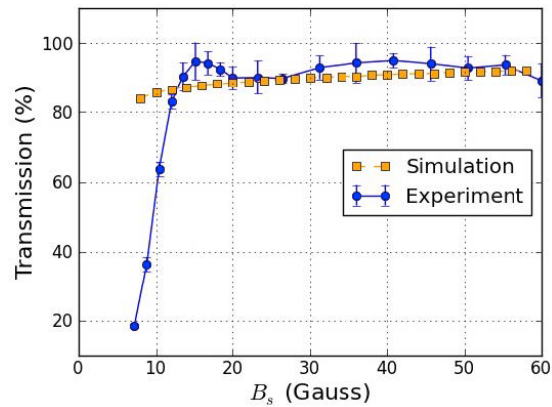

FIGURE 7. (left) high-permeability alloy spider used to terminate the field for electrostatic beam extraction; and (right) spider transmission.

To further analyze the performance of the magnetic spider in non-adiabatically extracted electrostatic beams with minimal perpendicular velocity kick, we proceeded to focus the resulting beams with the Einzel lens, using the collector cup (previously described) as our main diagnostic. Again, for small values of B_s performance was very poor, but for optimal conditions ($B_s = 50$ G) we were able to focus about 70% of a beam with initial radius 2.5 mm into the collector cup (see Fig. 8). About 10% particle loss is due to collisions with the spider metal.

These data are consistent with a magnification factor around 2, although it should be understood that as the beam is compressed spatially, transverse beam energy increases, so the beam has large divergence at the focus point. Preliminary simulations (still under development) support all the basic results just mentioned.
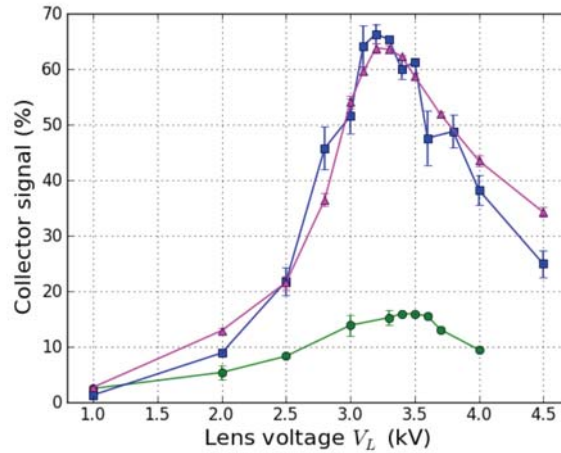

FIGURE. 8. Beam transmission through collector cup as a function of lens voltage V_L, presented for three different values of extraction field $B_s = 20$ (●), 50(■), and 80 G (▲). Note poor performance at $B_s = 20$ G probably due to asymmetry field resulting in residual beam angle w.r.t. apparatus, and that $B_s = 50$ G represents optimal performance because the initial beam radius decreases with increasing B_s.

The immediate focus of work will now be continued development of extraction through the high-permeability spider. It is planned to rebuild the beam line to include additional correction coils and alignment apparatus in the field transition region and immediately before the spider. The lens and collector system will also be rebuilt, optimizing the design based upon experience with the first generation apparatus. For example, previous experiments were hindered severely by not having the ability to scan the collector cup in the plane transverse to the beam direction and this will be rectified.

CONCLUDING REMARKS

Investigations are described here of new positron-beam formation techniques. The operation, optimization and limitations of cryogenic, trap-based beams were discussed. With simple extensions of this technique, it appears to be possible to achieve a beam with energy spread of ≤ 9 meV FWHM, produced using gas cooled to

~ 50 K, with the possibility of reaching 20 K using collisions with noble gas dimers. In a second area, progress is described to create higher quality electrostatic beams using a high-permeability spider. While promising, this approach will require additional attention to what appear to be small magnetic asymmetries near the spider that prevent non-adiabatic beam extraction at an optimally low magnetic field ~ 5 - 10 gauss.

Trap-based positron beam systems are now in place throughout the world. The new trap-based beam formation techniques described here, if successful, can be expected to be important in adding new capabilities to those positron beam facilities, and to new traps and trap-based beam systems as they come online.

ACKNOWLEDGEMENTS

REFERENCES

1. C.M. Surko, G.F. Gribakin, S.J. Buckman, *J. Phys. B: At. Mol. Opt. Phys.* **38**, R57 - R126 (2005).
2. D.W. Gidley, D.Z. Chi, W.D. Wang, R.S. Vallery, *Ann. Rev. Mat. Sci.* **36**, 49-79 (2006).
3. P.G. Coleman, *Positron beams and their applications*, (World Scientific, Singapore, 2000).
4. M. Charlton, J.W. Humberston, *Positron Physics*, (Cambridge Univ. Press, Cambridge, U. K., 2001).
5. G.F. Gribakin, J.A. Young, C.M. Surko, *Rev. Mod. Phys.* **82**, 2557 - 2607 (2010).
6. M. Amoretti, C. Amsler, G. Bonomi, A. Bouchta, P. Bowe, C. Carraro, C.L. Cesar, M. Charlton, M. Collier, M. Doser, V. Filippini, K. Fine, A. Fontana, M. Fujiwara, R. Funakoshi, P. Genova, J. Hangst, R. Hayano, M. Holzscheiter, L. Jorgensen, V. Lagomarsino, R. Landua, D. Lindelof, E.L. Rizzini, M. Macri, N. Madsen, G. Munuzio, M. Marchesotti, P. Montagna, H. Pruys, C. Regenfus, P. Riedler, J. Rochet, A. Rotondi, G. Rouleau, G. Testera, A. Variola, T. Watson, D. VanderWerf, *Nature* **419**, 456-459 (2002).
7. G. Gabrielse, N. Bowden, P. Oxley, A. Speck, C. Storry, J. Tan, M. Wessels, D. Grzonka, W. Oelert, G. Schepers, T. Sefzick, J. Walz, H. Pittner, T. Hansch, E. Hessels, *Phys. Rev. Lett.* **89**, 233401-233405 (2002).
8. G.B. Andresen, M.D. Ashkezari, M. Baquero-Ruiz, W. Bertsche, P.D. Bowe, E. Butler, C.L. Cesar, M. Charlton, A. Deller, S. Eriksson, J. Fajans, T. Friesen, M.C. Fujiwara, D.R. Gill, A. Gutierrez, J.S. Hangst, W.N. Hardy, R.S. Hayano, M.E. Hayden, A.J. Humphries, R. Hydomako, S. Jonsell1, S.L. Kemp, L. Kurchaninov, N. Madsen, S. Menary, P. Nolan, K. Olchanski, A. Olin, P. Pusa1, C.Ø. Rasmussen, F. Robicheaux, E. Sarid, D.M. Silveira, C. So, J.W. Storey, R.I. Thompson, D.P.v. derWerf, J. S.Wurtele, Y. Yamazaki, *Nature Physics* **7**, 558 (2011).
9. G. Gabrielse, R. Kalra, W. S. Kolthammer, R. McConnell, P. Richerme, D. Grzonka, W. Oelert, T. Sefzick, M. Zielinski, D.W. Fitzakerley, M.C. George, E.A. Hessels, C.H. Storry, M. Weel, A. Mullers, J. Walz, *Phys. Rev. Lett.* **108**, 113002 (2012).
10. D.B. Cassidy, A.P. Mills, Jr., *Nature* **449**, 195-197 (2007).
11. D.B. Cassidy, P. Crivelli, T.H. Hisakado, L. Liszkay, V.E. Meligne, P. Perez, H.W.K. Tom, A. P. Mills Jr, *Phys. Rev. A* **81**, 012715 (2010).
12. A.P. Mills, *Nucl. Instrum. Methods B* **192**, 107-116 (2002).
13. R.L. Wahl, in *Principles and Practice of Positron Emission Tomography*, (Lippincott, Williams and Wilkins, Philadelphia, PA, 2002).
14. D.B. Stout, A.F. Chatziioannou, T.P. Lawson, R.W. Silverman, S.S. Gambhir, M.E. Phelps,

Molecular Imaging and Biology **7**, 393-402 (2005).

15. P.J. Schultz, K.G. Lynn, *Rev. Mod. Phys.* **60**, 701-779 (1988).
16. S.J. Gilbert, C. Kurz, R.G. Greaves, C.M. Surko, *Appl. Phys. Lett.* **70**, 1944-1946 (1997).
17. A.P. Mills, *Appl. Phys.* **23**, 189 (1980).
18. C.M. Surko, R.G. Greaves, *Phys. Plasmas* **11**, 2333-2348 (2004).
19. T.J. Murphy, C.M. Surko, *Phys. Rev. A* **46**, 5696-5705 (1992).
20. R.G. Greaves, C.M. Surko, *Nucl. Instrum. Methods B* **192**, 90-96 (2002).
21. S. Marjanovic, M. Suvakov, A. Bankovic, M. Savic, G. Malovic, S. Buckman, Z. Petrovic, *IEEE Trans. Plas. Sci.* **39**, 2614-2615 (2011).
22. J.A. del Valle, F. A. Gianturco, *Phys. Chem. Chem. Phys.* **7**, 318 (2005).
23. J.R. Danielson, T.R. Weber, C.M. Surko, *Appl. Phys. Lett.* **90**, 081503 (2007).
24. T.R. Weber, J.R. Danielson, C.M. Surko, *Phys. Plasmas* **13**, 123502 (2008).
25. T.R. Weber, J.R. Danielson, C.M. Surko, *Phys. Plasmas* **16**, 057105 (2009).
26. A. David, G. Kogel, P. Sperr, W. Triftshauser, *Phys. Rev. Lett.* **87**, 067402 (2001).
27. A.P. Mills, *Applied Physics Letters* **37**, 667-668 (1980).
28. T.R. Weber, J.R. Danielson, C.M. Surko, *Phys. Plasmas* **17**, 123507, 123501 - 123510 (2010).
29. F.J. Mulligan, M.S. Lubell, *Measurement Science and Technology* **4**, 197-203 (1993).
30. W. Stoeffl, P. Asoka-Kumar, R. Howell, *Appl. Surf. Sci.* **149**, 1-6 (1999).